Lobe dynamics and space charge distribution in nonsteady electroconvection

A. T. Pérez
Departamento de Electrónica y Electromagnetismo, Facultad de Física. Avenida Reina Mercedes s/n, 41012 Sevilla, Spain

R. Chicón
Departamento de Física, Universidad de Murcia, Apartado 4021, Murcia 30071, Spain

A. Castellanos
Departamento de Electrónica y Electromagnetismo, Facultad de Física, Avenida Reina Mercedes s/n, 41012 Sevilla, Spain

(Received 1 July 1998)

This paper deals with chaotic charge transport in finite amplitude electroconvection. In steady finite amplitude electroconvection there is an inner region in the convection cell that remains free of charge. When the liquid velocity is time dependent, as it is always observed in experiments, this region is no longer free of charge. Lobe dynamics analysis is used to elucidate the mechanism of charge trapping. [S1063-651X(99)01101-0]

PACS number(s): 47.52.+j, 47.65.+a, 05.45.Gg

I. INTRODUCTION

Electroconvection in a liquid layer subjected to unipolar injection is a classical problem in electrohydrodynamics (EHD) because of its theoretical and practical importance [1–4]. In steady convective cells ions cannot enter the region where the downward vertical liquid velocity is larger than the upward ionic velocity. As a consequence, the cell is divided into two regions, one charged and the other empty of charge, separated by a boundary referred to as the separatrix.

However, that solution is unstable and it is not observed in the laboratory. In effect, for any fluctuation that increases the velocity field the separatrix moves across a charged region and, as a result, ions are trapped. These trapped ions modify the fluid motion since the latter is driven by an electrical torque that depends on the detailed spatial distribution of the ions in the cell. As a consequence, the dynamics of nonsteady finite amplitude electroconvection depends crucially on the trapping and detrapping of ions in the otherwise empty region. Due to the complexity of the ion distribution, the response of the fluid is also highly complex, thus making this problem not amenable to analytical solution and recourse to sophisticated numerical methods is needed [5].

The use of tools from the theory of dynamical systems, i.e., Poincaré maps and Melnikov functions, has given useful insights into partial aspects of this problem [6–8]. In those works it was shown that a small periodic velocity field superimposed on the velocity field of steady finite amplitude electroconvection gives rise to a chaotic distribution of charge. This chaotic mixing of charge is due to the heteroclinic tangle linked to the separatrix. Those studies were carried out under the assumption of weak injection and for values of the velocity field slightly above the ionic drift velocity.

In this work an additional tool, i.e., lobe dynamics [9], is used to obtain detailed information on the ion distribution in the cell. We consider liquid velocities much larger than the ionic drift velocity, which are typical of finite amplitude electroconvection. This has allowed us to determine whether or not an ion is going to be trapped depending on the injection site and time. Trapping occurs only on discrete portions (bands) of the injector that drift following the lobe motion. Also the statistics of trapped ions is better described using this technique. This is important to progress in our understanding of the coupling between the charge distribution and the velocity field.

II. STATEMENT OF THE PROBLEM

The geometry we consider in this paper is that of a liquid layer confined between two parallel metallic plates, separated a distance d. The liquid has permittivity ϵ, viscosity η, and density ρ. Ions in the liquid have a mobility K and injection of ions occurs from one of the plane electrodes, where the charge density is considered to be constant and of value q_0. Ions are removed from the system once they reach the opposite electrode, the collector. A voltage difference V is applied between the electrodes.

The charge density distribution that appears in the liquid at rest is potentially unstable. This can be easily understood considering the charge conservation equation

$$\frac{\partial q}{\partial t}+\nabla\cdot[q(K\boldsymbol{E}+\boldsymbol{u})]=0, \tag{1}$$

where q is the charge density, $\boldsymbol{E}$ the electric field, and $\boldsymbol{u}$ the liquid velocity. Using Poisson's equation

$$\nabla\cdot\boldsymbol{E}=\frac{q}{\epsilon}, \tag{2}$$

Eq. (1) can be set

$$\frac{dq}{dt}=-\frac{K}{\epsilon}q^2, \tag{3}$$

where $d/dt\equiv\partial/\partial t+(K\boldsymbol{E}+\boldsymbol{u})\cdot\nabla$ is the total derivative along a charge carrier path.

Equation (3) is readily integrated to give

$$q=\frac{q_0}{1+Kq_0t/\epsilon}. \tag{4}$$

Therefore, the charge density decreases along a charge carrier trajectory and hence decreases from the injector. This is a potentially unstable situation, analogous to that of a liquid layer heated from below, the Rayleigh-Bénard problem.

The linear stability analysis was done several years ago [1,10] and three nondimensional parameters appear:

$$T=\frac{\epsilon V}{K\eta}, \quad C=\frac{q_0d^2}{\epsilon V}, \quad M=\frac{1}{K}\sqrt{\frac{\epsilon}{\rho}}. \tag{5}$$

T represents the ratio of the destabilizing Coulomb force to the stabilizing viscous force, C is a measure of the injection strength, and M is the ratio of the hydrodynamic mobility to the ionic mobility. For weak injection $C\ll 1$, the liquid is set into motion for $TC^2\geqslant 222$, whereas for a space charge limited current ($C\gg 1$) the instability threshold is $T=160$.

A nonlinear stability analysis has already been done [2]. We recall here the main issues of this analysis restricted to the weak injection case. The mechanical equations may be written in a nondimensional form, taking as units for distance, potential, charge density, and velocity d, V, $\epsilon V/d^2$, and KV/d, respectively. The Navier-Stokes equation is then

$$\frac{T}{M^2}\left(\frac{\partial \boldsymbol{u}}{\partial t}+\boldsymbol{u}\cdot\boldsymbol{\nabla}\boldsymbol{u}+\boldsymbol{\nabla}p\right)=\nabla^2\boldsymbol{u}+Tq\boldsymbol{E}, \tag{6}$$

where the last term is the Coulomb force. The fluid motion is assumed to be in the form of a two-dimensional roll $\boldsymbol{u}=A\boldsymbol{u}_0$, where $\max|\boldsymbol{u}_0|=1$. Choosing a coordinate system such that the injecting electrode coincides with the plane $z=0$, the stream function Ψ is taken as

$$\Psi=\frac{L}{2\pi}[1-\cos(2\pi z)]\sin\left(\frac{\pi x}{L}\right) \tag{7}$$

such that

$$u_{0x}=\frac{\partial\Psi}{\partial z}, \tag{8a}$$

$$u_{0z}=-\frac{\partial\Psi}{\partial x}, \tag{8b}$$

where L is the half wavelength obtained from the linear stability analysis. Multiplying Eq. (6) by $\boldsymbol{u}_0$, integrating over the cross section of a roll, and neglecting the time derivatives, i.e., in the viscous regime, we arrive at the following relation between the amplitude A and the parameter T:

$$A=-T\frac{\int q\boldsymbol{u}_0\cdot\boldsymbol{E}\,dx\,dz}{\int(\boldsymbol{u}_0\cdot\nabla^2\boldsymbol{u}_0)\,dx\,dz}, \tag{9}$$

where the integral in the numerator is a function of A through Eq. (1). For the evaluation of this integral it is most convenient to analyze first the major features of the ion trajectories. These trajectories are the solutions of the system of ordinary differential equations

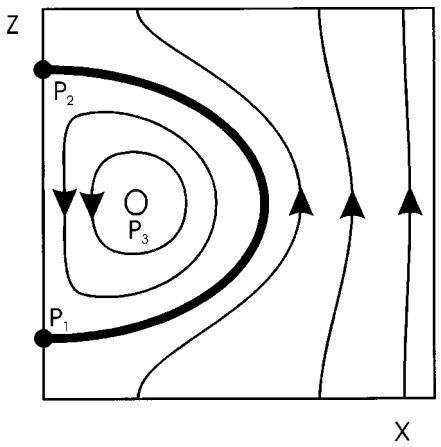

FIG. 1. Phase portrait of the system in Eq. (11) for $A>1$. In all figures, x and z are dimensionless, as defined in Sec. II.

$$\frac{d\boldsymbol{r}}{dt}=A\boldsymbol{u}_0+\boldsymbol{E}. \tag{10}$$

In the weak injection case Coulomb repulsion can be neglected and the electric field may be approximated by $\boldsymbol{E}=\boldsymbol{e}_z$, the unit vector in the z direction. Equation (10) can then be written in the form of the Hamilton equations

$$\frac{dx}{dt}=\frac{\partial H}{\partial z}, \tag{11a}$$

$$\frac{dz}{dt}=-\frac{\partial H}{\partial x}, \tag{11b}$$

with $H=-x+A\Psi(x,z)$.

Some typical ion trajectories, which give an overall view of the phase portrait of the system, are plotted in Fig. 1 for $A>1$ (the nondimensional ionic drift velocity equals unity). There are three equilibrium points P_1, P_2, and P_3. P_1 and P_2 are saddle points whereas P_3 is a center. The bold line is called the separatrix, or heteroclinic, and inside this line the backward velocity of the liquid is greater than the ionic drift velocity. Ions cannot enter this region which remains free of charge. The separatrix separates an outer region where $q=C$ and an inner region where $q=0$. Equation (9) is then

$$A=-TC\frac{\int_{\Omega_2}u_{0z}dx\,dz}{\int(\boldsymbol{u}_0\cdot\nabla^2\boldsymbol{u}_0)dx\,dz}, \tag{12}$$

where Ω_2 is the outer region. This expression can be transformed using Eqs. (8) into

$$A^2=\frac{TCS(A)}{\int(\boldsymbol{u}_0\cdot\nabla^2\boldsymbol{u}_0)dx\,dz}, \tag{13}$$

$S(A)$ being the area of the inner region. When $A\to\infty$ the separatrix tends to the borders of the cell and $S(A)\to L\times 1$, giving the asymptotic behavior

$$A^2\propto TC. \tag{14}$$

On the other hand, for $A\sim 1$ the separatrix is an ellipse and

$$S(A)=\frac{\sqrt{6}L(A-1)}{2\pi A}. \tag{15}$$

By substituting this last relationship into Eq. (13) it is found that T, as a function of A, reaches a minimum value T_f for $A=1.6$ and that $T_f=0.93T_cC$, where T_c is the linear stability threshold [4]. This minimum value represents a nonlinear threshold of stability. Thus a hysteresis loop appears: Increasing TC^2 gives no motion until one reaches the linear stability limit. Then the motion starts with a finite value of $A>1$. Decreasing TC^2, the motion does not cease until the value of the nonlinear stability limit is reached.

Experiments [11,12] show that the liquid motion is always time dependent and chaotic in nature. An attempt to understand this feature was carried out in [6], where the behavior of the carrier trajectories under periodic perturbations of a steady roll, i.e., $A(t)=A_0+\varepsilon\sin\omega t$, was studied for the weak injection case. The existence of the so-called heteroclinic tangle was proved, generating a chaotic separatrix layer and therefore leading to a chaotic behavior of the system.

More recently a numerical algorithm has been developed, based on a superparticle method, that has been able to reproduce all the characteristics of electroconvection, even the chaotic behavior in weak and strong injection [5]. The present paper is complementary to that work. Here we use a tool of the theory of dynamical systems, lobe dynamics, to analyze in more detail the ion trajectories in nonsteady electroconvection. We first introduce the fundamental concepts of lobe dynamics in the case of a periodic perturbation. Then we extend the analysis to pseudoperiodic perturbations, as an intermediate step before going to the more complex, but realistic, case of a chaotic signal $A(t)$ supplied by the numerical simulation. Finally, we consider the problem of the suppression of Hamiltonian chaos when Coulomb repulsion is not negligible.

III. POINCARÉ MAP, HETEROCLINIC TANGLE, AND LOBE DYNAMICS

A. Periodic perturbation

Let us consider the system given in Eq. (10) with $A(t)=A_0+\varepsilon\sin\omega t$. Since the flow is unsteady, there exists the possibility of having chaotic trajectories. Even a simple and regular flow may induce a very complex charge distribution. This is due to the breaking of the separatrix, which gives rise to the so-called heteroclinic tangle and stretches and folds the trajectories. The type of mixing so produced is different from molecular or turbulent diffusion and it has been referred to as laminar chaotic mixing [13].

Two dynamical tools are very useful in the study of chaotic mixing: the Poincaré map and Melnikov's function. First, the nonautonomous system

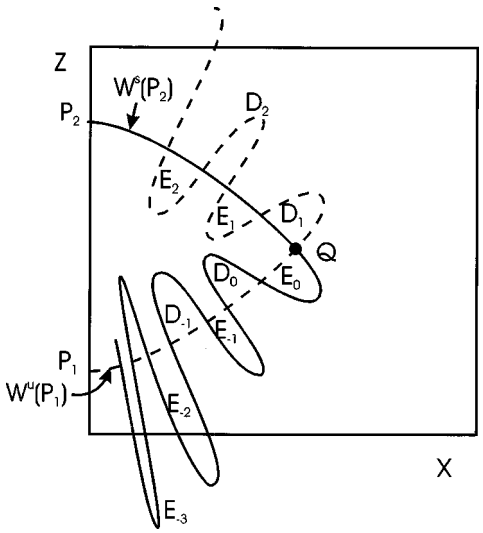

FIG. 2. Invariant manifolds, heteroclinic tangle, and lobe dynamics for a periodic perturbation.

$$\frac{dx}{dt}=A(t)u_{0x}+E_x, \tag{16a}$$

$$\frac{dz}{dt}=A(t)u_{0z}+E_z \tag{16b}$$

is converted to the equivalent suspended autonomous system

$$\frac{dx}{dt}=A(\theta)u_{0x}+E_x, \tag{17a}$$

$$\frac{dz}{dt}=A(\theta)u_{0z}+E_z, \tag{17b}$$

$$\frac{d\theta}{dt}=1. \tag{17c}$$

Time periodicity permits one to identify the planes $\theta=0$ and $\theta=T_0$, with $T_0=2\pi/\omega$, so that a cylindrical state space $R^2\times S^1$, where $S^1=[0,T_0)$ is the circle, is considered. We define a cross section $\Sigma_{t_0}=\{(x,z,\theta)\,|\,\theta=t_0\}$ and the Poincaré map

$$P_\varepsilon:\quad \Sigma_{t_0}\to\Sigma_{t_0}, \tag{18}$$

$$P_\varepsilon(x(t_0),z(t_0))=(x(t_0+T_0),z(t_0+T_0)). \tag{19}$$

In this way the Poincaré map of the flow is obtained by associating with a point at a fixed phase of the periodic perturbation its location under the evolution by the dynamical equations after a period of the perturbation.

While points P_1 and P_2, which are hyperbolic, are fixed points of the Poincaré map (technically speaking, they are robust) the point P_3 may disappear under nonconservative perturbations [14], i.e., it is not a robust feature of the system. However, if the perturbation is conservative, P_3 remains a fixed point of the Poincaré map. Neither is the separatrix robust. It may break under perturbation. In addition, there exist invariant manifolds W^u and W^s associated with the saddle points. Referring to Fig. 2, $W^s(P_2)$ is the set of

pointsthat tend to P_2 when $t\to\infty$ and $W^u(P_1)$ is the set of points that tend to P_1 when $t\to-\infty$.

Melnikov's function is defined as

$$M(t_0)=\int_{-\infty}^{\infty}[f_1(\mathbf{r}_s(t))g_2(\mathbf{r}_s(t),t+t_0) - f_2(\mathbf{r}_s(t))g_1(\mathbf{r}_s(t),t+t_0)]dt, \tag{20}$$

where the dynamical equations have been written in the form

$$\frac{dx_1}{dt}=f_1(x_1,x_2)+\varepsilon g_1(x_1,x_2,t), \tag{21a}$$

$$\frac{dx_2}{dt}=f_2(x_1,x_2)+\varepsilon g_2(x_1,x_2,t) \tag{21b}$$

and $\mathbf{r}_s(t)$ is the unperturbed separatrix. Melnikov's function permits one to compute the distance between the manifolds at any point on the separatrix $(x_1(-t_0),x_2(-t_0))$ through

$$d(t_0)=\varepsilon\frac{M(t_0)}{|\mathbf{f}(\mathbf{r}_s(-t_0))|}+O(\varepsilon^2). \tag{22}$$

Here t_0 parametrizes the distance along the unperturbed separatrix (see [9] for details).

When Melnikov's function has simple zeros the two manifolds $W^u(P_1)$ and $W^s(P_2)$ intersect transversely. For a perturbation of the form $\mathbf{g}(\mathbf{r},t)=\sin(\omega t)\mathbf{G}(\mathbf{r})$, Melnikov's function can be expressed as

$$M(t_0)=F(\omega)\sin\omega t_0, \tag{23}$$

which means that the two manifolds intersect transversely each period of the perturbation. Obviously the image by P_ε of any intersection point is another intersection point.

Lobes are defined as regions bounded by segments of the two manifolds connecting two consecutive intersection points [9]. Lobes map onto one another at each iteration of P_ε. Referring to Fig. 2, E_{-3} maps onto E_{-2}, which maps onto E_{-1}, which maps onto E_0, which maps onto E_1. Similarly, D_{-1} maps onto D_0, which maps onto D_1, etc. For a conservative system all the lobes have the same area. Unless otherwise stated, our discussion applies to the weak injection case, so the system can be considered conservative.

We define the inner region as one bounded by segments of $W^u(P_1)$ and $W^s(P_2)$ that intersects at point Q. This point Q may be any of the intersection points of the two manifolds. All the points in lobe E_0, and only those points, enter the inner region after one iteration of the Poincaré map. Conversely, all the points in lobe D_0 leave the inner region at the next iteration. As the invariant manifolds intersect at an infinity of points, a lobe E_i intersects an infinity of lobes D_j. The number of iterations in which a point is trapped in the inner region depends on these successive intersections and it is very sensitive to the initial position of the point in the lobe. For a complete discussion of the details of lobe dynamics, the reader is referred to the paper by Rom-Kedar *et al.* [9].

Let us now return to the physical problem of charge transport. Our system is confined by the two electrodes. In other fluid mechanics problems the physical boundaries do not intersect the lobes since a usual condition is that velocity vanishes at the walls. However, this is not the case in our problem. Although the velocity of the liquid *does* vanish at the electrodes, the ions drift velocity is nonzero *even* at the electrodes. This turns out to be an important distinctive feature of the electroconvection problem and many of its main characteristics are determined by the intersections of the electrodes with the lobes. Namely, charges injected at the intersections of the electrode with the lobes will become trapped inside the inner region, whereas those injected outside the lobes will travel directly from the injecting to the collecting electrode.

In order to make more quantitatively precise the previous qualitative conclusions, we define the residence time $R(x_0,t_0)$ as the number of iterations of the Poincaré map that a particle injected at a point x_0 at a time t_0 needs to reach the collector. As a consequence of the previous discussion, a band structure for $R(x_0,t_0)$ as a function of x_0, with t_0 fixed, is to be expected. The value of $R(x_0,t_0)$ is very sensitive to small changes in x_0. This sensitivity is due to the fact that a lobe intersects an infinity of other lobes in the inner region. Figure 3 is intended to illustrate this situation. In Fig. 3(a) a particle is injected inside a lobe at location 1, gets into the inner region after three iterations, gets out after six iterations, and finally reaches the collector after ten iterations. Another particle injected very close to the previous one would follow the path shown in Fig. 3(b), reaching the collector after eleven iterations. Finally, in Fig. 3(c) we show the path of a particle that travels directly from the injector to the collector without being trapped in the inner region.

We have computed the residence time $R(x_0,0)$ as a function of the abscissa x_0 of the point of injection, solving numerically Eq. (10) with $A(t)=A_0+\varepsilon\sin\omega t$. The values chosen for the parameters are $A_0=10.5$, $\varepsilon=0.1$, and $T_0=0.2$ in order to compare with the results that will be discussed below for a chaotic signal $A(t)$ obtained from numerical simulation under typical conditions of weak injection. Figure 4 reveals the band structure in the residence time.

The Poincaré map can be defined for different values of the initial phase of the perturbation. All the maps so obtained are topologically equivalent, but the actual position of the lobes drifts when t_0 is varied. Due to the periodicity of the perturbation, the lobes undergo a complete displacement to occupy the position of the next lobe in the sequence when t_0 varies from 0 to T_0. Referring to Fig. 2 again, the lobe denoted E_{-3} becomes the lobe E_{-2} and so on. As a consequence of lobe drift, for any value of x_0 in a certain interval around the origin, there should be an interval $(t_1,t_2)\subset[0,T_0)$ such that particles injected at x_0 at times $t_0\in(t_1,t_2)$ will become trapped. To give a complete view of the dependence of the residence time with respect to their variables we have plotted $R(x_0,t_0)$ in Fig. 5. The values of $R(x_0,t_0)$ are scaled according to a gray scale: The darker the point the higher the residence time.

The properties of $R(x_0,t_0)$ reflect the lobe dynamics. A conspicuous characteristic of this function is self-similarity, responsible for the pattern visible in the trapping region. As the manifolds are invariant sets of the Poincaré map, their intersection is also an invariant set. This set has the structure of a Cantor set: Inside a lobe that intersects the injector, an infinity of lobes intersect, contained in one another. This is the cause of self-similarity.

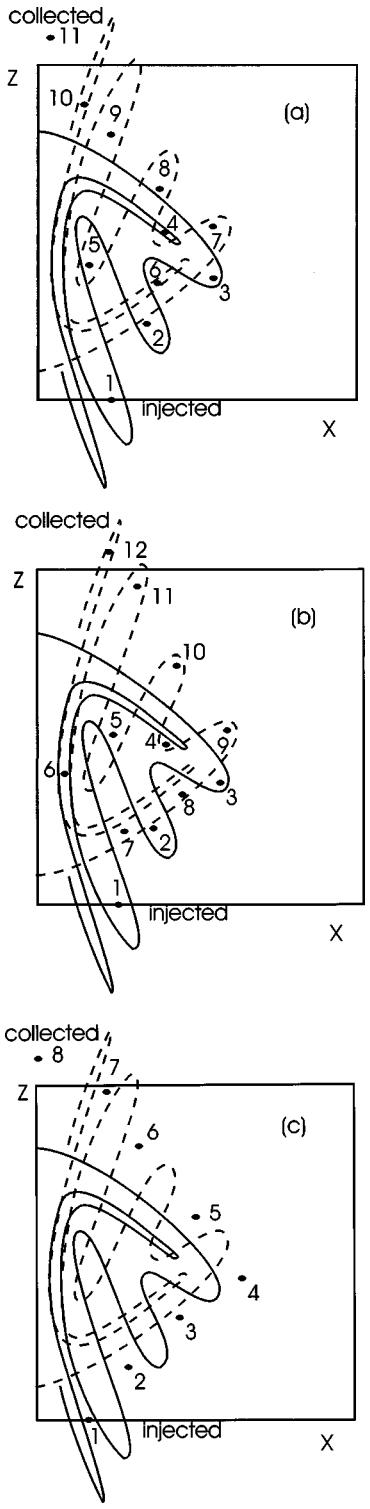

FIG. 3. Sensitivity of the residence time with respect to the injection point: (a) and (b) paths with trapping in the inner region (c) path without trapping.

The function $R(x_0,t_0)$ also provides a means for computing the fraction of charge inside the inner region. Let us define $R(x_0)=\min_{t_0\in[0,T_0)}R(x_0,t_0)$. This value represents the minimum number of iterations a particle needs to go directly from the injector to the collector. For instance, in Fig. 3(c) this number would be seven. Then $R(x_0,t_0)-R(x_0)$ is the number of iterations that a particle injected at

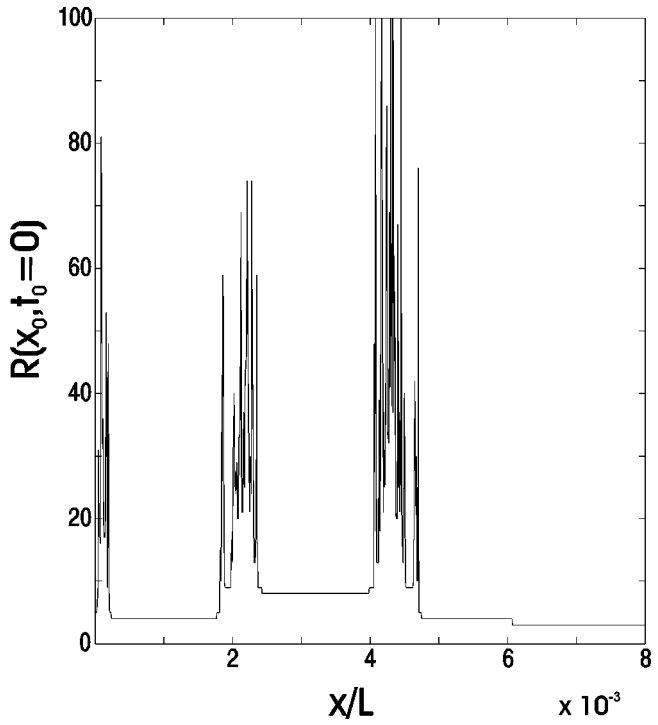

FIG. 4. Band structure of the residence time $R(x_0,t_0=0)$ as a function of x_0 for a periodic perturbation with $A_0=10.5$, $\varepsilon=0.1$, and $T_0=0.2$.

x_0 at time t_0 remains trapped in the inner region. Assuming that particles are being injected continuously, after many iterations we will have $R(x_0,t_0)-R(x_0)$ particles trapped in the inner region that were injected at x_0 and t_0-nT, n

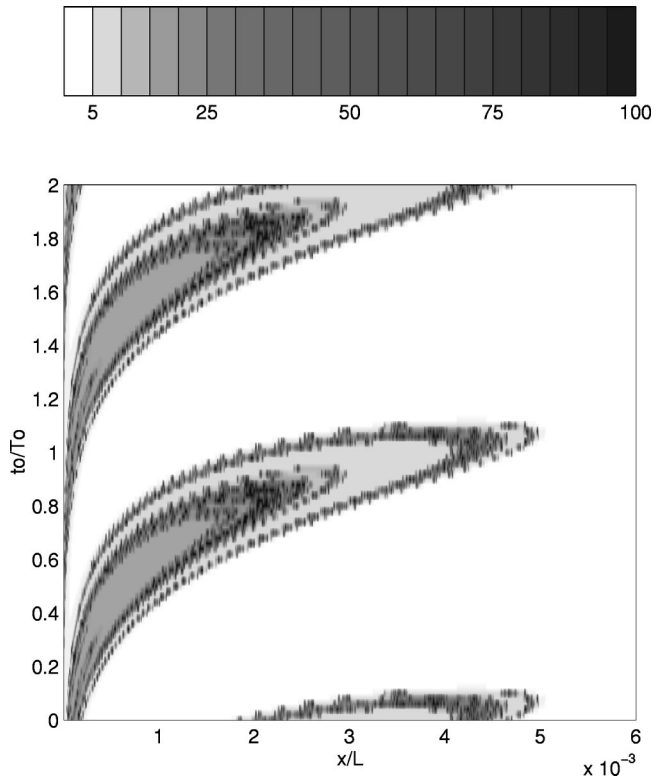

FIG. 5. Residence time $R(x_0,t_0)$ for a periodic perturbation with $A_0=10.5$, $\varepsilon=0.1$, and $T_0=0.2$. Note the periodicity with t_0.

$\in Z^+$. Summing for all $t_0 \in [0,T_0)$ yields the total number of trapped particles coming from x_0. Finally, summing for all $x_0 \in [0,L]$ we have, averaged over one period, the total number of trapped particles present in the system:

$$\hat{N} = \Sigma_{t_0} \Sigma_{x_0} (R(x_0,t_0) - R(x_0)). \tag{24}$$

On the other hand, the total number of particles in the cell volume, averaged over one period, is $N = \Sigma_{t_0} \Sigma_{x_0} R(x_0,t_0)$. The fraction of particles in the inner region is then

$$\beta = \frac{\Sigma_{t_0} \Sigma_{x_0} (R(x_0,t_0) - R(x_0))}{\Sigma_{t_0} \Sigma_{x_0} R(x_0,t_0)}. \tag{25}$$

For the parameters corresponding to Fig. 5 we obtain $\beta = 0.012$.

B. Pseudoperiodic perturbation

Before going to the case involving a continuous spectrum it would be worthwhile to analyze the simpler case of a pseudoperiodic perturbation. Beigie *et al.* [15] (see also [16]) have studied the lobe dynamics for quasiperiodic perturbations of dynamical systems. They study time-dependent perturbations that can be decomposed in several frequencies, that is,

$$g_i(t) = g_i(\omega_1 t, \omega_2 t, \ldots) \quad (i = 1,2). \tag{26}$$

The equivalent suspended system will be now

$$\frac{dx_1}{dt} = f_1(x_1,x_2) + \varepsilon g_1(x_1,x_2,\theta_1,\theta_2,\ldots), \tag{27a}$$

$$\frac{dx_2}{dt} = f_2(x_1,x_2) + \varepsilon g_2(x_1,x_2,\theta_1,\theta_2,\ldots), \tag{27b}$$

$$\frac{d\theta_1}{dt} = 1, \tag{27c}$$

$$\frac{d\theta_2}{dt} = 1, \tag{27d}$$

$$\vdots .$$

A Poincaré section can still be defined as

$$\Sigma_{\theta_{10}} = \{(x,z,\theta_1,\theta_2,\ldots) \,|\, \theta_1 = \theta_{10} \in [0,2\pi/\omega_1)\}, \tag{28}$$

but this section is no longer two dimensional. The corresponding Poincaré map P_ε is also defined. After one iteration of the map it is not only

$$(x(t_0),z(t_0)) \rightarrow (x(t_0+T_0),z(t_0+T_0)) \tag{29}$$

but also

$$\theta_2 \;\rightarrow\; \theta_2 + 2\pi \frac{\omega_2}{\omega_1}, \tag{30a}$$

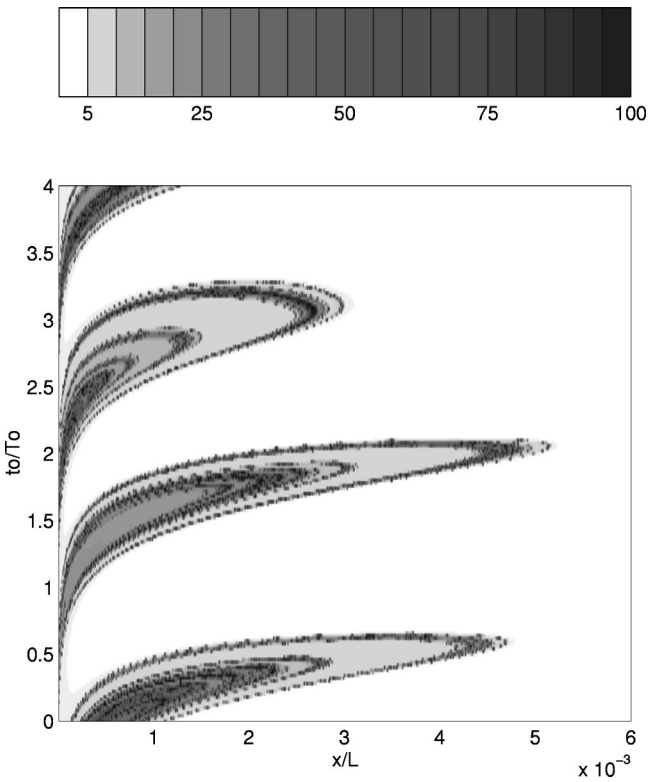

FIG. 6. Residence time $R(x_0,t_0)$ for a pseudoperiodic perturbation [Eq. (31)] with $A_0 = 10.5$ and $\varepsilon = 0.05$.

$$\theta_3 \;\rightarrow\; \theta_3 + 2\pi \frac{\omega_3}{\omega_1}, \tag{30b}$$

$$\vdots$$

where we have taken $T_0 = 2\pi/\omega_1$. Although the lobes structure still exists, it changes at each iteration of the map. Only if all the frequencies are commensurable would the lobe dynamics be periodic.

As the features of the residence time are consequence of the lobe dynamics, $R(x_0,t_0)$ is no longer expected to be a periodic function of t_0. We have computed $R(x_0,t_0)$ from the numerical solution of Eq. (10) with

$$A(t) = A_0 + \varepsilon(\sin \omega_1 t + \sin \omega_2 t). \tag{31}$$

For the purpose of comparison with the periodic perturbation we have chosen $A_0 = 10.5$, $\varepsilon = 0.05$, and the two frequencies related by $\omega_1/\omega_2 = g$ and $(\omega_1 + \omega_2)/2 = \omega_0$, where $\omega_0 = 2\pi/0.2$ is the angular frequency considered in the periodic case and $g = (\sqrt{5}-1)/2$ is the golden mean. The results obtained for the residence time are shown in Fig. 6. As it was expected, $R(x_0,t_0)$ retains the pattern consequence of a well defined lobe dynamics, but it is not a periodic function of t_0. The fraction β of trapped charge can be computed in the same way as before, but taking into account many periods of the base frequency. The value obtained for β differs from that obtained for the periodic perturbation only after the third significant digit. It should be noticed that the value of β depends on the strength of the perturbation. The result previously mentioned has been obtained when the maximum value is the same for the periodic and the pseudoperiodic

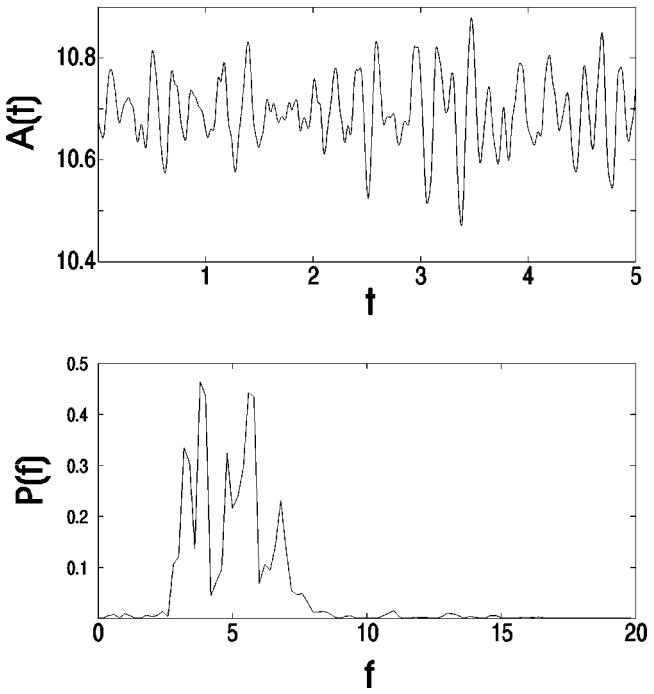

FIG. 7. (a) Time dependence and (b) power spectrum of a chaotic signal $A(t)$ obtained in the weak injection regime for $C=0.1$ and $T=25\,000$.

perturbations. Another possibility is choosing ε such that both perturbations have the same rms value. In this case we obtain $\beta=0.015$ for the pseudoperiodic perturbation, a value higher than for the periodic one.

C. Chaotic signal $A(t)$

Electroconvection due to unipolar injection is neither a steady phenomenon nor a periodic one. Numerical simulations [5] fit this feature. A typical time-dependent signal $A(t)$ is shown in Fig. 7, corresponding to a weak injection simulation with $C=0.1$ and $T=25\,000$. The power spectrum is continuous and shows a broadened peak around a central frequency $f=5$, which corresponds to a nondimensional period $T_0=0.2$.

The residence time $R(x_0,t_0)$ has been computed considering a Poincaré map corresponding to the central frequency of the peak. The calculation has been performed through the entire simulation of the EHD problem, without neglecting Coulomb repulsion between the ions. Therefore, the system is not strictly conservative because $\nabla\cdot\boldsymbol{E}=q>0$. However, for sufficiently small values of C this should not substantially modify the general features of the phase portrait [7].

The presence of many frequencies in $A(t)$ makes the results for the residence time, shown in Fig. 8, fairly different from those corresponding to a periodic perturbation. However, $R(x_0,t_0)$ retains a certain structure, far from periodic in the variable t_0. A given position in the injector will inject charge that will pass through trapping and nontrapping episodes, depending on the time of injection. The fraction of trapped charge is $\beta=0.0025$, which has been calculated considering several periods of the base frequency.

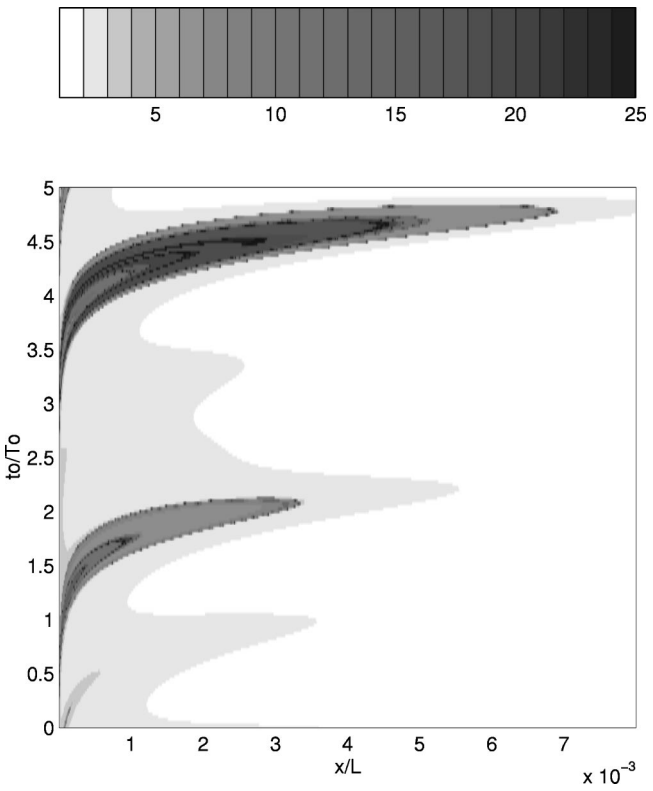

FIG. 8. Residence time $R(x_0,t_0)$ obtained from the amplitude $A(t)$ shown in Fig. 7.

IV. SUPPRESSION OF HAMILTONIAN CHAOS

Up to now we have focused on the weak injection regime and the dynamical system has been assumed to be strictly conservative, as in Secs. III A and III B, or approximately conservative as in Sec. III C. In [7] it was shown that when the injection strength C increases, so that Coulomb repulsion is no longer negligible, the heteroclinic tangle should disappear. The effect of Coulomb repulsion on the phase portrait of the system is shown in Fig. 9. Trajectories inside the inner region spiral out, finally reaching the collector through a narrow channel near $x=0$. No trajectory originating at the injector enters the inner region.

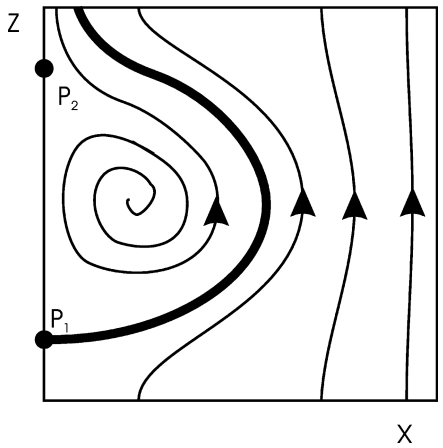

FIG. 9. Effect of Coulomb repulsion on the phase portrait. The inner region is connected with the collecting electrode through a narrow channel near $x=0$.

Melnikov's function when Coulomb repulsion is taken into account was found to be [7]

$$M(t_0)=F(\omega)(\sin\omega t_0-2C). \tag{32}$$

For $C>0.5$ the function has no zeros and the heteroclinic tangle disappears. The calculation leading to Eq. (32) was performed under the assumption $A\sim 1$. However, in the actual EHD problem the electroconvection regime is characterized by values of A appreciably higher than the ionic drift velocity, so that the threshold $C=0.5$ should be taken only as a rough estimation for the extinction of the heteroclinic tangle. Numerical simulation of the electroconvection for different values of C yields $C=0.2$ as the critical value above which the heteroclinic tangle ceases to exist. No trapping of charge carrier occurs above that value and no structure consequence of lobe dynamics is found any longer in the residence time $R(x_0,t_0)$.

The suppression of the Hamiltonian chaos does not result, however, in a steady electroconvection solution. On the contrary, the liquid velocity remains time dependent and of chaotic nature [5]. Although the analysis presented in this paper deepens our comprehension of EHD chaos in the weak injection case, this leaves the question of the ultimate origin of EHD chaos still open.

V. CONCLUSION

In this paper we have analyzed the mechanisms that determine the charge distribution in nonsteady finite amplitude electroconvection. Lobe dynamics, a recent concept tied to chaotic mixing in dynamical systems, has been applied to the cases of periodic and nonperiodic velocity amplitudes. In the periodic case, there is a band structure in the injecting electrode, so that points inside certain intervals of the abscissa inject particles that become trapped in the inner region. This band structure changes periodically with the time of injection. In the nonperiodic case, there remains a certain band structure that is not periodic. The fraction of trapped charge in a convective cell is computed from the residence time of the particles. A critical value has been found for the injection strength, above which Coulomb repulsion is strong enough to destroy the band structure. These ideas provide some insight into the origin of the chaotic nature of electroconvection due to unipolar injection.

ACKNOWLEDGMENT

This work was carried out with financial support under Contract No. PB96-1375 from DGICYT.

[1] P. Atten and R. Moreau, J. Mec. **11**, 471 (1972).
[2] P. Atten and J. C. Lacroix, J. Mec. **18**, 469 (1979).
[3] A. Castellanos and P. Atten, IEEE Trans. Ind. Appl. **IA23**, 825 (1987).
[4] A. Castellanos, IEEE Trans. Electr. Insul. **26**, 1201 (1991).
[5] R. Chicón, A. Castellanos, and E. Martín, J. Fluid Mech. **344**, 43 (1997).
[6] A. T. Pérez and A. Castellanos, Phys. Rev. A **44**, 6659 (1991).
[7] R. Chacón, A. T. Pérez, and A. Castellanos, Phys. Rev. E **49**, 1756 (1994).
[8] A. T. Pérez, R. Chacón, and A. Castellanos, Int. J. Bifurcation Chaos Appl. Sci. Eng. **6**, 2627 (1996).
[9] V. Rom-Kedar, A. Leonard, and S. Wiggins, J. Fluid Mech. **214**, 347 (1990).
[10] J. M. Schneider and P. K. Watson, Phys. Fluids **13**, 1948 (1970).
[11] P. Atten, J. C. Lacroix, and B. Malraison, Phys. Lett. **79A**, 255 (1980).
[12] B. Malraison and P. Atten, Phys. Rev. Lett. **49**, 723 (1982).
[13] J. M. Ottino, *The Kinematics of Mixing: Stretching, Chaos, and Transport* (Cambridge University Press, Cambridge, 1989).
[14] A. T. Pérez and A. Castellanos, Phys. Rev. A **40**, 5844 (1989).
[15] D. Beigie, A. Leonard, and S. Wiggins, Nonlinearity **4**, 775 (1991).
[16] S. Wiggins, *Chaotic Transport in Dynamical Systems* (Springer-Verlag, New York, 1992).